Journal of Power Sources 194 (2009) 1120–1127

Contents lists available at ScienceDirect

Journal of Power Sources

journal homepage: www.elsevier.com/locate/jpowsour

Electrochemical corrosion of Pb–1 wt% Sn and Pb–2.5 wt% Sn alloys for lead-acid battery applications

Wislei R. Osório*, Leandro C. Peixoto, Amauri Garcia

Department of Materials Engineering, State University of Campinas – UNICAMP, PO Box 612, 13083-970 Campinas, SP, Brazil

ARTICLE INFO

Article history:
Received 15 May 2009
Received in revised form 14 June 2009
Accepted 15 June 2009
Available online 24 June 2009

Keywords:
As-cast Pb–Sn alloys
Lead-acid battery
Cellular array
Electrochemical impedance
Corrosion resistance

ABSTRACT

The aim of this study was to compare the electrochemical corrosion behavior of as-cast Pb–1 wt% Sn and Pb–2.5 wt% Sn alloy samples in a 0.5 M H_2SO_4 solution at 25 °C. A water-cooled unidirectional solidification system was used to obtain the as-cast samples. Electrochemical impedance spectroscopy (EIS) diagrams, potentiodynamic polarization curves and an equivalent circuit analysis were used to evaluate the electrochemical corrosion response. It was found that a coarse cellular array has a better electrochemical corrosion resistance than fine cells. The pre-programming of microstructure cell size of Pb–Sn alloys can be used as an alternative way to produce as-cast components of lead-acid batteries with higher corrosion resistance associated with environmental and economical aspects.

1. Introduction

A variety of grid manufacturing processes [1–3] have been used by many battery manufacturers to decrease battery grid weight as well as to reduce the production costs, and to increase the battery life-time cycle and the corrosion resistance [3,4]. A battery grid must be dimensionally stable and have mechanical properties which can resist the stresses of the charge/discharge reactions without bending, stretching or warping. Pb–Sn, Pb–Sb and Pb–Ca–Sn alloys are commonly used in the production of positive and negative grids, connectors, posts and straps components of both VRLA – valve-regulated lead acid and SLI – starting, lighting and ignition which are widely applied in automotive and telecommunication services [1–3]. It is known that antimony enhances electrolysis of water into hydrogen and oxygen during charging, leading to water or electrolyte loss [4–7]. Pb–Sn and Pb–Sn(Ca) alloys can be better alternatives for the production of Pb-acid battery grids with a view to achieve a maintenance-free condition [4–11].

It is well known that the properties of battery grids are highly dependent on alloying content. In this context, the effects of alloying additions have been studied for a wide range of alloy compositions. Calcium additions of about 0.03 wt% are made in order to improve the resulting mechanical properties. However, due to its segregation to grain boundaries and interdendritic regions it can considerably affect the corresponding corrosion resistance in the paste adhesion and curing. Tin addition is in a range between 0.3 and 1.5 wt% [4,5,10] and it has a complex role on the kinetics of formation, passivation and growth rates of PbO and PbO_2 layers, as reported by Rocca and Steinmetz [12].

It is well known that the resulting cellular or dendritic microstructure array spacing has a strong influence on the overall surface corrosion resistance of binary alloys [13–18]. It is known that low growth rates during solidification and/or low alloy solute content can favor the growth of regular cell morphologies [15–18]. It was found that the improvement on the corrosion resistance depends on the cooling rate imposed during solidification which affects microstructural morphology and solute redistribution, and on the electrochemical behavior of solute and solvent [13–18].

Razaei and Damiri [7] reported that the control of solidification variables has an important role on the electrochemical behavior of lead-acid battery grid alloys. It was verified that lower cooling rates imposed during solidification of a Pb–Sb alloy casting provided antimony segregation to the interior of the casting, while surface antimony concentrations had significantly decreased.

Peixoto et al. [18] and Osório et al. [15] reported that coarse cellular samples were associated with better electrochemical corrosion resistance than fine cellular samples when considering experimental studies with Pb–Sn and Pb–Sb alloys subjected to corrosion tests in a 0.5 M H_2SO_4 solution.

The control of solidification variables with a view to pre-programming the resulting microstructure of as-cast components of binary lead alloys should be considered as an important alternative tool for the improvement of the resulting mechanical properties and electrochemical corrosion response. The present study aims to

* Corresponding author. Tel.: +55 19 3521 3320; fax: +55 19 3289 3722.
E-mail address: wislei@fem.unicamp.br (W.R. Osório).

0378-7753/$ – see front matter © 2009 Elsevier B.V. All rights reserved.
doi:10.1016/j.jpowsour.2009.06.051

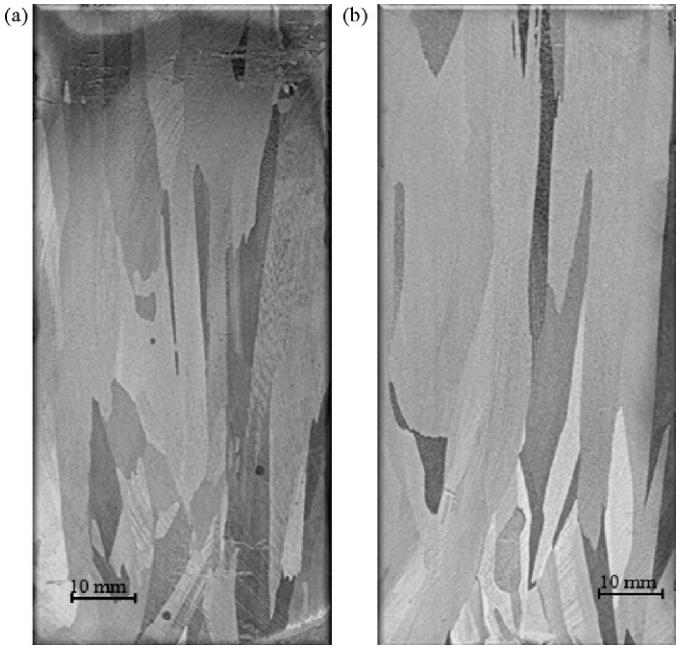

Fig. 1. Typical directionally solidified macrostructure of (a) Pb–1 wt% Sn and (b) Pb–2.5 wt% Sn alloys castings.

contribute to the development of correlations between microstructure and properties, by assessing the influence of the resulting microstructural morphology of as-cast Pb–1 wt% Sn and Pb–2.5 wt% Sn alloys on the general electrochemical corrosion behavior in a 0.5 M H_2SO_4 solution at 25 °C.

2. Experimental procedure

2.1. Specimens preparation

Pb–1 wt% Sn and Pb–2.5 wt% Sn alloys were prepared by using commercially pure metals: Pb (99.89 wt%) and Sn (99.99 wt%). The mean impurities were Fe (0.12%), Si (0.05%), Cu (0.015%), besides other elements with concentration less than 50 ppm.

A water-cooled unidirectional solidification system was used in the experiments. The solidification set-up was designed in such way that the heat was extracted only through the water-cooled bottom, promoting vertical upward directional solidification. From the water-cooled bottom to the top of the unidirectionally solidified casting a wide range of cooling rates were obtained since the efficiency of heat extraction decreases with the distance from the bottom of the casting. Such thermal behavior affects cells spacing along the casting length. Temperatures were monitored via type J thermocouples (made from 0.2 mm wire and sheathed in 1.6 mm diameter stainless steel tubes). More details concerning this solidification set-up can be obtained in previous articles [13,15,16].

As-cast specimens were sectioned from the center of the casting, ground, polished and etched to reveal the macrostructure (the etchant was a mixture of aqueous solutions: 3:1 – in volume – HNO_3 solution and 6:1 – in volume – ammonium molybdate). The samples were polished and etched by using a 37 cm^3 glacial acetic acid and 15 cm^3 of hydrogen peroxide solution at room temperature for microscopy examination. The microstructural characterization was carried out by using an optical microscope associated with an image processing system Neophot 32 (Carl Zeiss, Esslingen, Germany) and Leica Quantimet 500 MC (Leica Imaging Systems Ltd., Cambridge, England) [15–18].

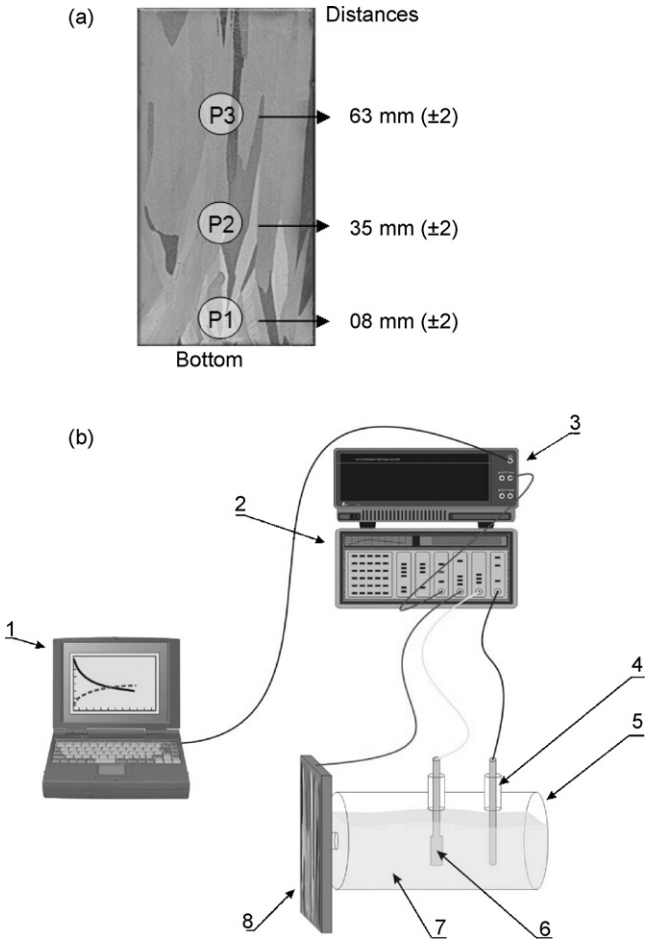

Fig. 2. Schematic representations of (a) positions along the casting from where the samples for corrosion tests were collected and (b) personal computer and software to data measurements (1), frequency analyzer (2), potentiostat (3), reference electrode (4), glass cell kit (5), platinum counter-electrode (6), 0.5 M H_2SO_4 electrolyte solution (7), and Pb–Sn alloy work-electrode (8).

2.2. Electrochemical corrosion tests

In order to evaluate and compare the electrochemical corrosion behavior of the Pb–1 wt% Sn and Pb–2.5 wt% Sn alloy samples, electrochemical corrosion tests were performed in a 1 cm^2 circular area of ground (600 grit SiC finish) sample surfaces. Electrochemical impedance spectroscopy (EIS) measurements began after an initial delay of 30 min for the samples to reach a steady-state condition. The tests were carried out with the samples immersed in a stagnant and naturally aerated 500 cm^3 of a 0.5 M H_2SO_4 solution at 25 °C (pH = 0.88 ± 0.05), used to simulate the battery electrolytic fluid. A potentiostat (EG & G Princeton Applied Research, model 273A) coupled to a frequency analyzer system (Solartron model 1250), a glass corrosion cell kit with a platinum counter-electrode and a saturated calomel reference electrode (SCE) were used to perform the EIS tests. The potential amplitude was set to 10 mV at open-circuit, peak-to-peak (AC signal), with 5 points per decade and the frequency range was set from 100 mHz to 100 kHz. The samples were further ground to a 1200 grit SiC finish, followed by distilled water washing and air drying before measurements.

Potentiodynamic measurements were also carried out in the aforementioned solution at 25 °C using a potentiostat at the same positions where the EIS tests were carried out. These tests were conducted by stepping the potential at a scan rate of 0.2 mV s^{-1} from −0.800 mV (SCE) to +2800 mV (SCE) at open-circuit. Using an automatic data acquisition system, the potentiodynamic polarization

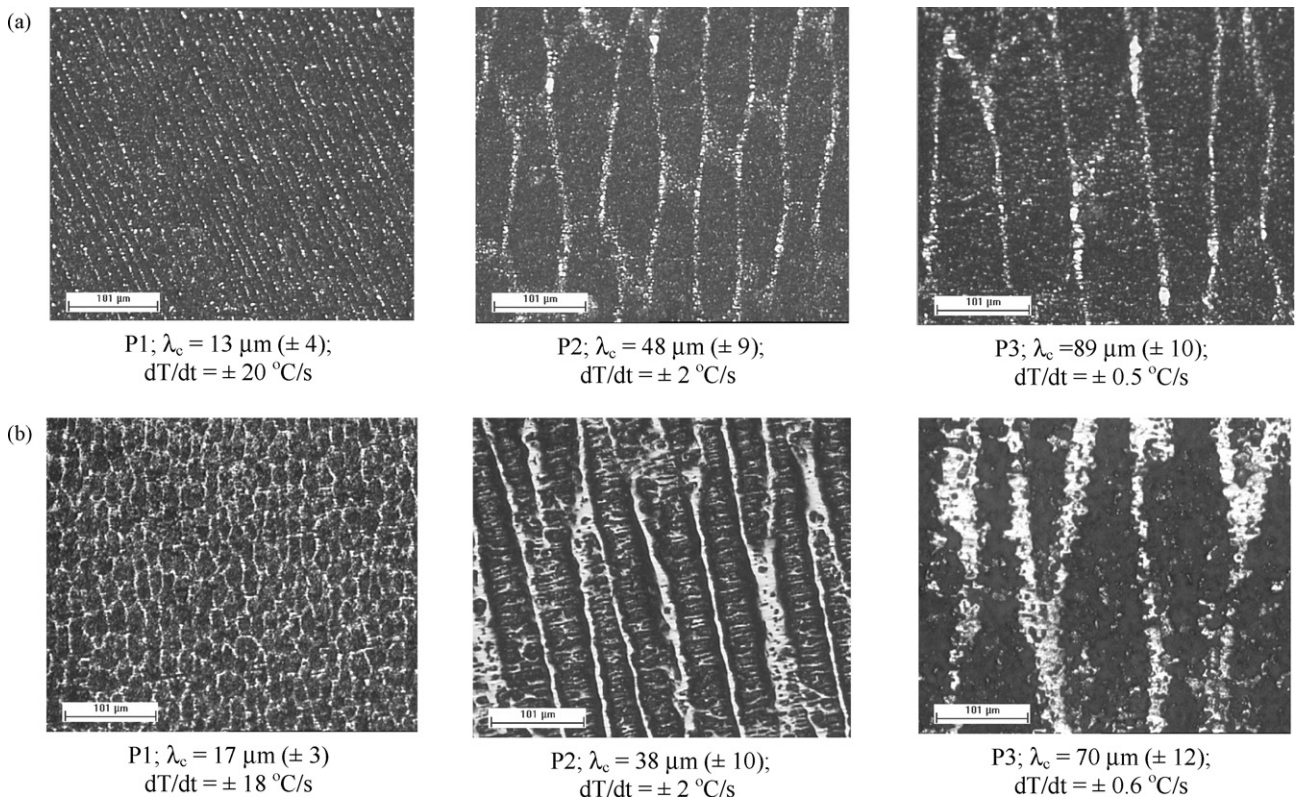

Fig. 3. Typical cellular morphologies along the casting length at positions P1 (8 mm), P2 (35 mm) and P3 (63 mm) from the bottom of the casting and its corresponding average cellular spacings and cooling rate for (a) Pb–1 wt% Sn and (b) Pb–2.5 wt% Sn alloy castings (optical magnification: 125×).

curves were plotted and both corrosion rate and potential were estimated by Tafel plots by using both anodic and cathodic branches at a scan rate of 0.2 mV s^{-1} from −250/+250 mV (SCE) at open-circuit (corresponding to −1200 and −700 mV *vs*. MSE). Although the SCE electrode is not commonly used in lead-acid system studies, a SCE electrode can also be used as a reference electrode since the one inconvenient is the fact that chloride may contaminate the electrolyte, and other is to convert from SCE to MSE or other potential scales (ASTM G3).

Duplicate tests for EIS and potentiodynamic polarization curves were carried out. In order to supply quantitative support for discussions on these experimental EIS results, an appropriate model (ZView version 2.1b) for equivalent circuit quantification has also been used.

It is important to remark that the corrosion behavior analysis of the present work differs from studies of PbO/PbO_2 formation which consider the corrosion of the lead electrode and proceed at much higher potentials. The analysis also differs from studies of $PbSO_4$ membrane layer formed on the electrode surface which in a 0.5 M H_2SO_4 solution presents high solubility, as detailed in the literature [19–21].

3. Results and discussion

3.1. Resulting as-cast microstructures

Fig. 1(a) shows the resultant directionally solidified casting macrostructures for both Pb–1 wt% Sn and Pb–2.5 wt% Sn alloys. It can be seen that the growth of columnar grains prevailed along the entire casting length due to the water-cooled unidirectional system, as similarly reported in other previous studies [15–17].

The positions along the casting from where the samples for corrosion tests were collected are shown by a schematic representation in Fig. 2(a). The potentiostat coupled to a frequency analyzer system, personal computer and corrosion cell kit are depicted in Fig. 2(b).

Typical microstructures observed along the cross-sections of both the Pb–1 wt% Sn and Pb–2.5 wt% Sn alloy castings are shown in Fig. 3(a) and (b), respectively. The as-cast microstructure consists of a completely cellular array, constituted by a Pb-rich matrix α-phase: solid solution of Sn in Pb with a eutectic mixture formation in the intercellular regions. The Pb-rich cellular matrix is depicted by dark regions with the intercellular eutectic mixture being represented by light regions.

A water-cooled mold imposes higher values of cooling rates near the casting/chill surface (bottom) and a decreasing profile along the casting length (top) due to the increase of the thermal resistance of the solidified shell with distance from the cooled surface, as reported in previous articles [15–17]. This influence translates to the observed experimental cellular spacing, with fine spacings close to the casting cooled surface (position P1) and coarser ones far from it (position P3). Average cooling rates (dT/dt) for positions P1, P2 and P3 are also shown in Fig. 3. Considering six (06) samples of Pb–1 wt% Sn and Pb–2.5 wt% Sn alloys, an experimental representation of cooling rate as a function of the cellular spacing can be made, as shown in Fig. 4. The line represents an empirical power law which fits the experimental points and average values of cellular spacing along with the standard variation are also presented. Similar cooling rates for both Pb–1 wt% Sn and Pb–2.5 wt% Sn alloy samples are clearly observed. Both alloys can be considered as dilute Pb–Sn alloys which can be contributed to this similar thermal behavior.

3.2. Electrochemical parameters

In the present investigation, both a potentiodynamic polarization method and a qualitative electrochemical technique were used

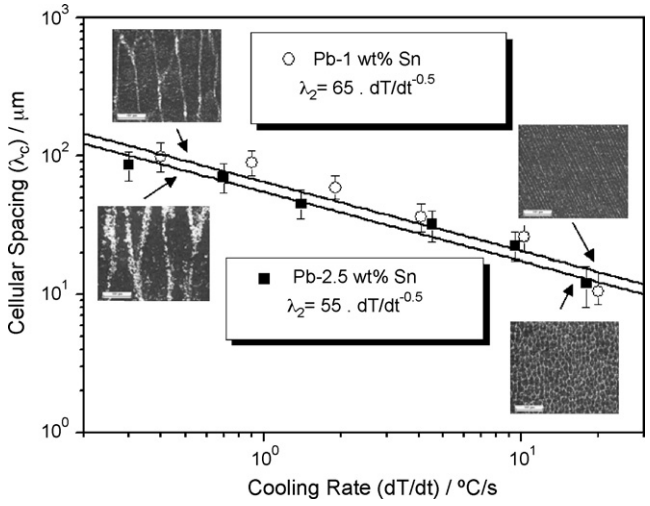

Fig. 4. Average cellular spacing as a function of cooling rate for both the Pb–1 wt% Sn and Pb–2.5 wt% Sn alloys castings.

to provide a consistent and useful way to investigate the tendency of the corrosion resistance.

Fig. 5 depicts the Bode and Bode-phase diagrams representing the modulus of impedance and phase angle as a function of

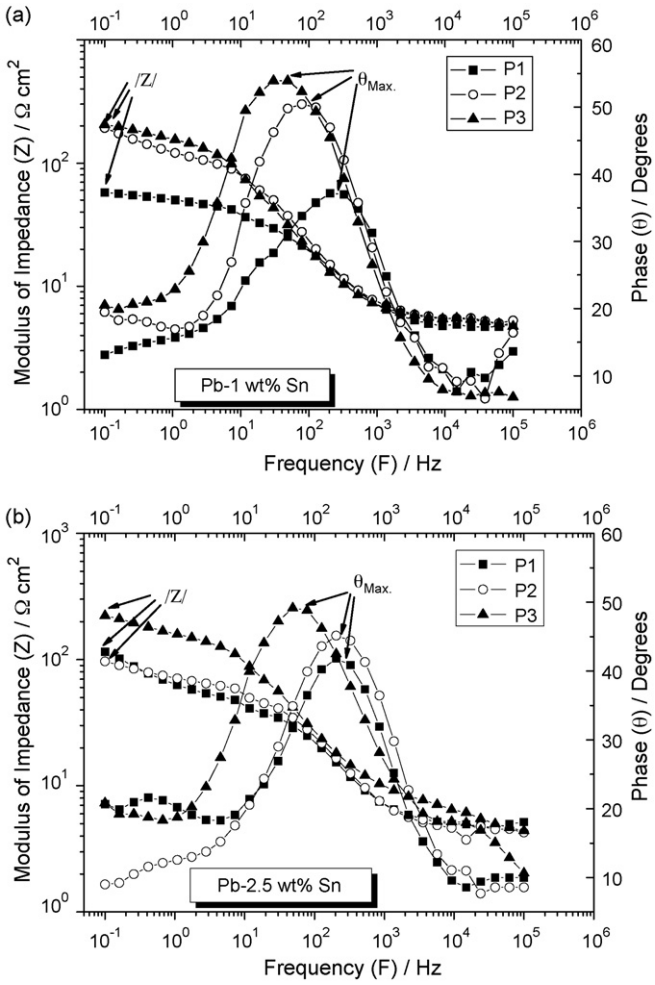

Fig. 5. Experimental EIS diagrams (*Bode and Bode-phase*) of (a) Pb–1 wt% Sn alloy and (b) Pb–2.5 wt% Sn alloy at positions P1, P2 and P3 in a 0.5 M H_2SO_4 solution at 25 °C.

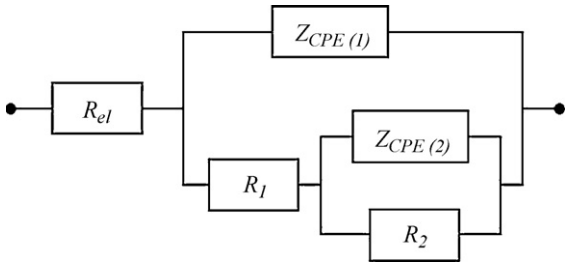

Fig. 6. Equivalent circuit used to obtain impedance parameters with the ZView® software.

frequency. The Bode-phase results indicate that two time constants can be associated with the corrosion kinetics of cellular array and intercellular region of Pb–Sn alloys. At a frequency range of 10^4–10^5 Hz, the first time constant which can be related with the reaction between the electrolyte and the tin-rich phase in the intercellular region is clearly observed. At low frequencies, in a range from 0.1 to 10 Hz, the second time constant appears and can be correlated with the reaction with the Pb-rich matrix.

It is known that at low frequency, Bode plot provides the maximum modulus of impedance (|*Z*|). In this context, at a frequency of 0.1 Hz, the cellular arrays of the Pb–1 wt% Sn alloy at positions P1, P2 and P3 have |*Z*| values of about 60, 180 and 210 Ω cm^2, respectively. The cellular arrays of the Pb–2.5 wt% Sn alloy at the same positions (P1 to P3) have |*Z*| values of about 110, 100 and 225 Ω cm^2, respectively. Considering the Bode-phase diagrams, maximum phase angles ($\theta_{max.}$) of about 55° in a frequency of 40 Hz and 50° in 60 Hz are observed for positions P3 of the Pb–1 wt% Sn and Pb–2.5 wt% Sn alloy samples, respectively. These experimental impedance parameters provide clear indications that the coarse cellular arrays of both the Pb–1 wt% Sn and Pb–2.5 wt% Sn alloys can be related to better electrochemical behavior when compared to the results which correspond to the fine cellular array. At frequencies between 10 and 10^3 Hz, interpretation of the nature and double electronic formation can be made [22].

An equivalent circuit analysis has also been conducted, which is similar to those developed in some previous articles [22–31]. Fig. 6 shows the proposed equivalent circuit used to fit the experimental data. The impedance parameters obtained by the ZView® software, are shown in Tables 1 and 2. The fitting quality was evaluated by chi-squared (χ^2) values of about 12×10^{-3} to 80×10^{-3} [26–31] for both Pb–1 wt% Sn and Pb–2.5 wt% Sn alloy samples, as shown in Tables 1 and 2.

The interpretation of the physical elements of the proposed equivalent circuit is similar to those reported in previous studies [13–18]. Thus, R_{el} is the electrolyte resistance, R_1 is the charge transfer resistance and R_2 stands for a polarization resistance due to the participation of adsorbed intermediates. $Z_{CPE(1)}$ and $Z_{CPE(2)}$ denote the double layer capacitance and the capacitance associated with the polarization resistance R_2. The parameters n_1 and n_2 are correlated with the phase angle, varying between −1 and 1.

Table 1
Impedance parameters obtained by the ZView® software fitting experimental and simulated results for Pb–1 wt% Sn alloy samples in a 0.5 M H_2SO_4 solution at 25 °C.

Parameters	P1	P2	P3
R_{el} (Ω cm^2)	4.1	5.2	5.4
$Z_{CPE(1)}$ (μFcm^{-2})	303 (±30)	316 (±31)	360 (±36)
$Z_{CPE(2)}$ (mFcm^{-2})	14 (±1)	11 (±1)	12 (±1)
n_1	0.73	0.77	0.81
n_2	0.28	0.81	0.52
R_1 (Ω cm^2)	33	119	170
R_2 (Ω cm^2)	100	160	1500
χ^2	77×10^{-3}	12×10^{-3}	32×10^{-3}

Table 2
Impedance parameters obtained by the ZView® software fitting experimental and simulated results for Pb–2.5 wt%Sn alloy samples in a 0.5 M H_2SO_4 solution at 25 °C.

Parameters	P1	P2	P3
R_{el} (Ω cm^2)	4.9	4.3	5.8
$Z_{CPE(1)}$ (μFcm^{-2})	155 (±15)	200 (±20)	350 (±35)
$Z_{CPE(2)}$ (mFcm^{-2})	14 (±1)	18 (±1)	12 (±1)
n_1	0.85	0.80	0.77
n_2	0.38	0.43	0.60
R_1 (Ω cm^2)	30	49	160
R_2 (Ω cm^2)	1386	1400	1439
χ^2	15×10^{-3}	11×10^{-3}	80×10^{-3}

The impedance of a constant phase element is defined as $Z_{CPE} = [C(j\omega)^n]^{-1}$ [26–31], where C is the capacitance; j is the current; ω is the frequency and $-1 \leq n \leq 1$. The value of n seems to be also associated with the non-uniform distribution of current as a result of roughness and surface defects [15–18,26–31].

Simulated and experimental results in Nyquist plots of the Pb–1 wt% Sn and Pb–2.5 wt% Sn alloy samples in sulfuric acid solution are shown in Fig. 7(a) and (b), respectively. All complex plane plots (Nyquist diagrams) are characterized by a capacitive arc at high frequencies (between 10^5 and 1 Hz) followed by a slope of about 45° at frequencies lower than 1 Hz [32,33], as also observed by Li et al. [34]. These Nyquist plots reveal that the diameters of the capacitive arcs for the coarse cellular region (position P3) are higher than those for fine cellular regions (positions P2 and P1).

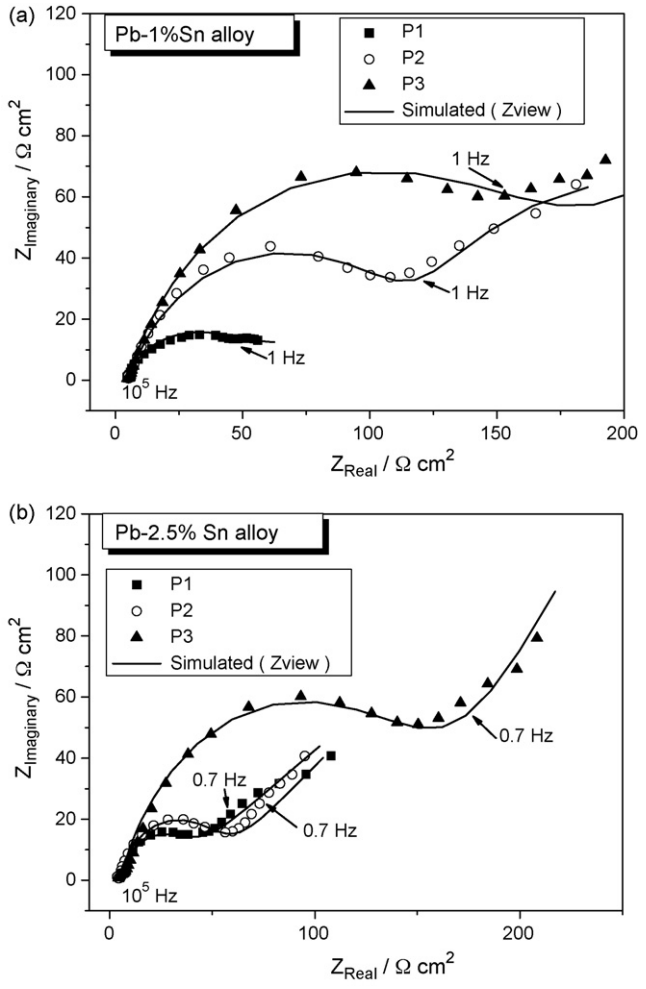

Fig. 7. Experimental and simulated Nyquist results for (a) Pb–1 wt% Sn and (b) Pb–2.5 wt% Sn alloys in a 0.5 M H_2SO_4 solution at 25 °C.

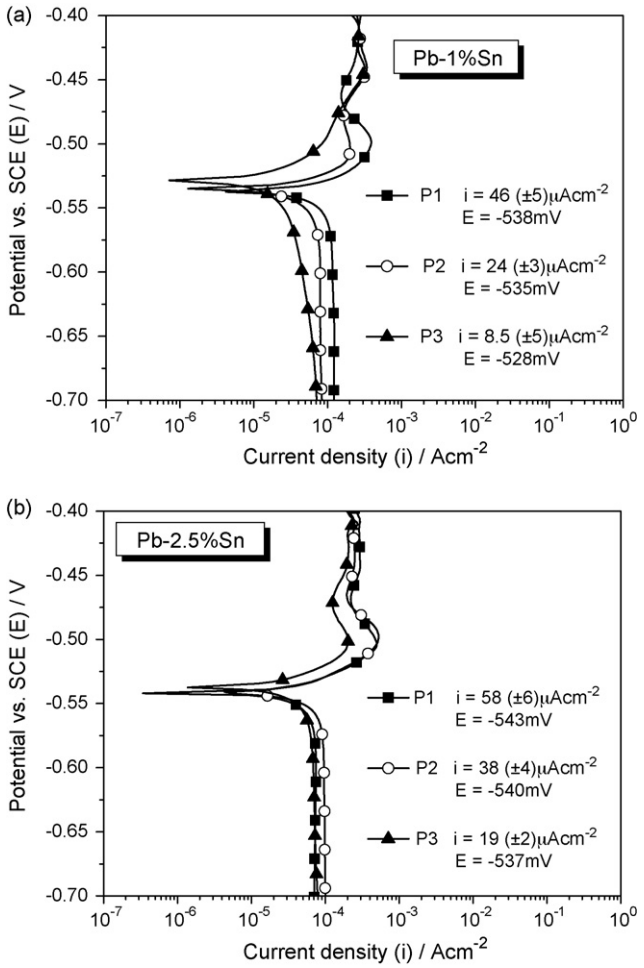

Fig. 8. Potentiodynamic polarization curves exhibiting current densities and corrosion potentials for (a) Pb–1 wt% Sn and (b) Pb–2.5 wt% Sn alloys samples in a 0.5 M H_2SO_4 solution at 25 °C.

These results show a similar tendency when compared to those analyzed in Bode and Bode-phase plots, shown in Fig. 3(a).

In Tables 1 and 2, it can be observed that R_2 is higher than R_1, which is an indication that R_2 has an important role on the electrochemical corrosion resistance of dilute as-cast Pb–Sn alloys. Assis et al. [27] observed similar trend in a study of Ti–Al alloys. These electrochemical impedance parameters also indicate that the coarse cellular array has better electrochemical corrosion resistance than the fine cellular structure.

The impedance parameters $Z_{CPE(2)}$ and R_2 closely correspond to that of adsorbed intermediates (e.g. $PbSO_4$, PbOH, etc.). As $Z_{CPE(2)}$ is similar for each position and each Pb–Sn alloy, the parameters R_1 and R_2 evidence that coarser cellular arrays have higher corrosion resistance than finer ones. R_1 corresponds to the polarization resistance and high values indicate better corrosion resistance. On the other hand, $Z_{CPE(1)}$ corresponds to the capacitance of double electronic formation at the surface of the Pb–Sn alloys samples and high values also indicate better electrochemical corrosion response.

Fig. 8(a) and (b) shows potentiodynamic polarization curves (from −0.7 to −0.4 V *vs.* SCE) for the Pb–1%Sn and Pb–2.5% Sn alloy samples at three different positions (P1, P2 and P3) corresponding to tests carried out in a 0.5 M H_2SO_4 solution at 25 °C. The corrosion current density (i_{corr}) was obtained from Tafel plots using both the cathodic and anodic branches of the polarization curves. These results reinforce the corrosion resistance tendency observed previously with the results of EIS and impedance parameters

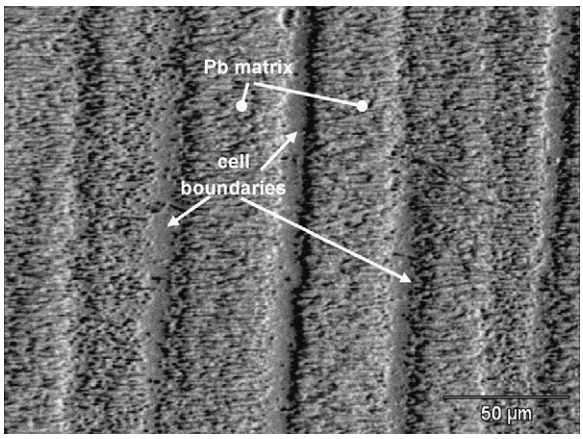

Fig. 9. (a) Typical SEM micrograph of a Pb–2.5 wt% Sn alloy sample after corrosion test (polarization).

(equivalent circuit), i.e., better electrochemical corrosion resistance being associated with coarser (position P3) Pb–Sn alloys cellular microstructures.

Considering the Pb–1 wt% Sn alloy, a current density of about 46 (±5) μA cm^{-2} associated with a corrosion potential of about −538 mV (SCE) is observed for position P1 (08 mm; λ_c = 15 μm). At positions P2 (35 mm; λ_c = 50 μm) and P3 (63 mm; λ_c = 80 μm), current densities and corrosion potentials of about 24 (±5) μA cm^{-2}; −535 mV (SCE) and 8.5 (±5) μA cm^{-2}; −528 mV (SCE) are attained. On the other hand, the Pb–2.5 wt% Sn alloy has similar corrosion potential at the three positions examined along the casting length (of about −540 mV, SCE) and current densities decreasing with increasing positions from P1 to P3 which are 58 (±6), 38 (±4) and 19 (±2) μA cm^{-2}, respectively. Fig. 9 evidences that the corrosion action is stronger at the cell boundaries, and as a result finer cell regions will be subjected to more generalized corrosion due to the more extensive boundaries distribution, which are typical of these refined regions.

During non-equilibrium solidification, the α-phase (Pb-rich) will have an increasingly Sn content from the cell center towards the cell boundaries, i.e., the intercellular regions, up to the eutectic composition, as shown in Fig. 10. The eutectic mixture (point #2) will be formed by alternated Pb-rich and Sn-rich phases giving rise to galvanic cell formation. Coarser cells tend to improve the corrosion resistance of dilute Pb–Sn alloys mainly due to the reduction of cellular boundaries which are regions of higher energy. It is well known that low solute content is one of the main factors favoring the formation of a cellular structure during solidification [35]. Generally, in a conventional casting or in a continuous casting of Pb alloys grids, refined cellular structures are produced [3–8]. The present experimental results have indeed shown that coarser cells tend to improve the corrosion resistance of Pb–1 wt% Sn and Pb–2.5 wt% Sn alloys mainly due to the reduction of cellular boundaries. This condition provides a better galvanic protection when compared to a fine microstructure cellular array. Fine cells will induce a more extensive corrosion action, being more susceptible to galvanic degradation. A similar tendency was also reported by Rosa et al. [16] and Osório et al. [15,17] in studies of corrosion resistance of Pb–Sb alloys in a 0.5 M H_2SO_4 solution. Peixoto et al. [18] have also reported higher electrochemical corrosion resistance for coarse equiaxed cells (λ_c = 200 μm) compared to fine equiaxed cells (λ_c = 25 μm) for Pb–1 wt% Sn alloy samples tested in a 0.5 M H_2SO_4 solution. Similar tendency of corrosion resistance was also observed for pure metals with fine and large equiaxed grains [15–18,36].

Comparison of electrochemical corrosion resistances of Pb–1 wt% Sn and Pb–2.5 wt% Sn alloys permits to assess the role of

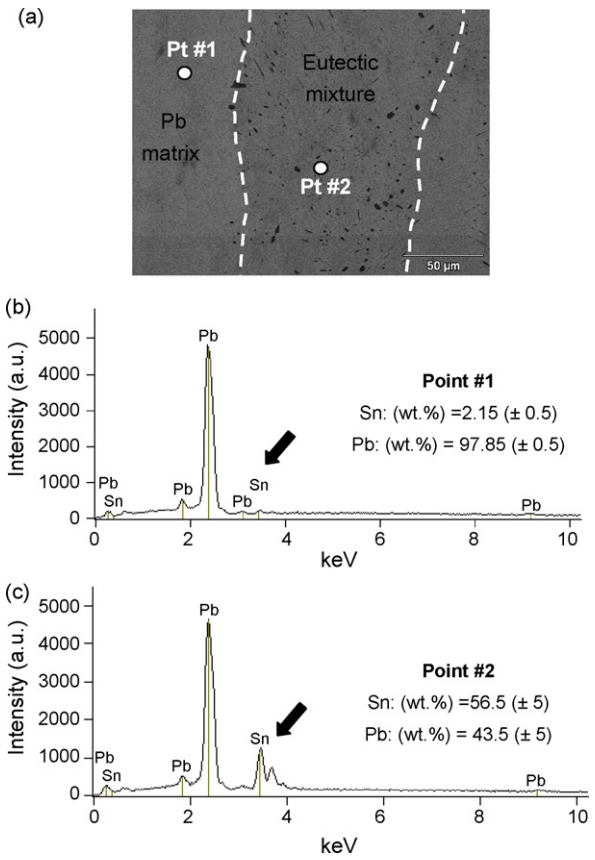

Fig. 10. (a) Typical SEM micrograph of a Pb–2.5 wt% Sn alloy evidencing the Pb-rich phase (point #1); (b) the eutectic mixture (point #2), and (c) the EDAX results with average chemical compositions for points #1 and #2.

tin content on the electrochemical behavior of Pb–Sn alloys. Simon et al. [37] reported that a Pb–1 wt% Sn alloy has better corrosion resistance than a Pb–2.5 wt% Sn alloy. The experimental impedance parameters, current density and corrosion potential obtained in the present study are in agreement with such conclusion reported by Simon et al. [37]. Fig. 11 shows a comparison of experimental current density as a function of cellular spacing for the Pb–1 wt% Sn and Pb–2.5 wt% Sn alloys giving indications of higher corrosion resistance for the latter alloy. Average current density with the

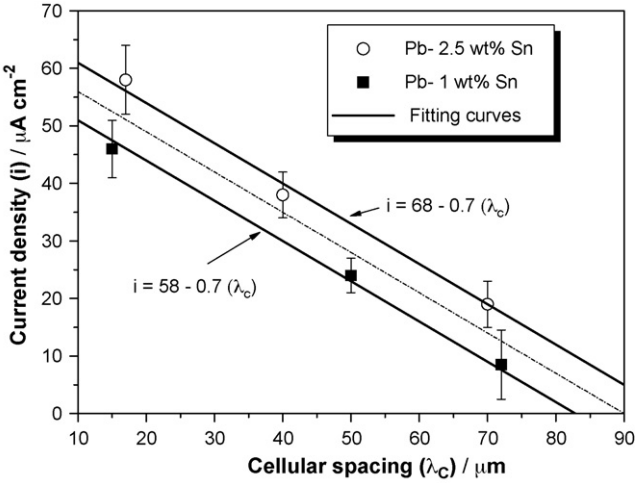

Fig. 11. Experimental current density as a function of cellular spacing for Pb–1 wt% Sn and Pb–2.5 wt% Sn alloys samples in a 0.5 M H_2SO_4 solution at 25 °C.

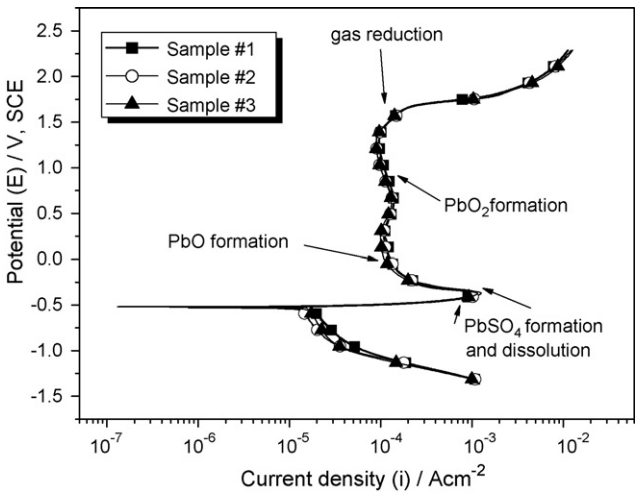

Fig. 12. Experimental anodic potentiodynamic polarization curves for three Pb–1 wt% Sn alloy samples in a 0.5 M H_2SO_4 solution at 25 °C.

standard variation is presented. The line represents an empirical power law which fits the experimental points.

Fig. 12 shows the experimental anodic potentiodynamic polarization curves for three different samples of the Pb–1 wt% Sn alloy in a 0.5 M H_2SO_4 solution at 25 °C.

Pavlov et al. [19–21] suggested that the open-circuit potential of the Pb–1 wt% Sn alloys is something lower than that of pure lead (−0.58 V, SCE) due to the accelerated self-discharge related to lower hydrogen overvoltage on the Sn electrode. At potentials above −0.95 V (Hg/Hg_2SO_4 or *vs.* MSE – *Mercury-mercurous Sulphate Electrode*) which corresponds to range between −580 and −540 mV (SCE), anodic oxidation of Pb takes place and Pb (II) ions are formed, as can be observed in Fig. 12. However, it is known that the rate of anodic oxidation of Pb to Pb (II) ions at this aforementioned range of potentials is not the process that determines the corrosion rate of lead in sulfuric acid. In addition to the anodic oxidation of lead, at potentials above −0.45 V (*vs.* MSE) or −0.08 V (*vs.* SCE) another anodic process begins in which Sn oxidation to Sn (II) and Sn (IV) can be involved.

A partial stabilization on current density is observed at about 10^{-3} A cm^{-2} between potentials −0.42 and −0.32 V (SCE) or +0.70 and −0.04 V (MSE). This indicates precipitation and dissolution mechanisms of $PbSO_4$ particles, as also verified in a previous study [18]. It is important to remark that the solubility of $PbSO_4$ in 0.5 M H_2SO_4 is relatively high and only small amounts of $PbSO_4$ crystals will be formed and reduced (dissolution–precipitation mechanism). Some $PbSO_4$ crystals are formed at the electrode surface which, after long enough polarization will form a semi-permeable membrane which, on turn, will passivate the electrode surface. A $PbSO_4$ membrane layer will be formed on the electrode surface (passivation) but not any PbO particle because a high and strong passivation for this formation is demanded [18–21].

At a potential region between −0.70 and −0.40 V (SCE), as shown in Fig. 8, the current depends on the spot the sample was taken from (the *P* value). However, at potentials above −0.20 V this dependence practically disappears evidencing that the three studied Pb–Sn alloy samples have similar $Pb/PbO/PbSO_4$ and Pb/PbO_2 electrode system formation. It can be said that the cellular array is the determinant factor influencing the corrosion action until the formation of electrode systems $PbO/PbSO_4$ and PbO/PbO_2. After this, the electrochemical behaviors of the different Pb–Sn samples experimentally examined, are very similar and connected to the oxide layer growth.

At potentials between −0.2 V and +0.4 V (SCE) and between +0.4 V and +1.5 V (SCE) of the $Pb/PbO/PbSO_4$ and the Pb/PbO_2 electrode systems, regions of stability are attained. Stabilizations in the current densities (of about 1.3×10^{-4} and 1.4×10^{-4} A × cm^{-2}) at a potential of about −0.08 V (SCE) (−0.45 V, MSE) are observed, which corresponds to PbO formation. In a range of current densities from 90 to 100 μA cm^{-2} associated with potentials between +1.06 and +1.30 V (SCE), reactions of PbO_2 formation can occur. Pavlov and its collaborators have systematically detailed these reactions [19–21].

Considering a conventional manufacturing of lead-acid battery components, the high cooling rates which are associated with the casting process will induce a deleterious effect on the general electrochemical corrosion response for dilute Pb–Sn alloys. In this context, the control of as-cast cellular microstructures can be used as an alternative way to produce as-cast components with reasonable corrosion resistance.

It is well known that a number of grid manufacturing processes [1–3] have been used in order to decrease battery grid weight as well as to reduce the production costs for applications in automotive and telecommunication fields as VRLA or SLI batteries [1–4]. As the electrochemical corrosion behavior of the Pb–1 wt% Sn and Pb–2.5 wt% Sn alloys are very similar when a same order of magnitude of the cellular array is considered, the production of battery components using Pb–2.5 wt% Sn alloy can considerably decrease the final battery weight. The production costs for 1 ton of each dilute Pb–Sn alloys are similar. However, a flat grid of Pb–2.5 wt% Sn alloy in an automotive battery has of about 2–3 g lower than a grid manufactured with a Pb–1 wt% Sn alloy. Considering that a pole of an automotive battery has of about 16 flat plates (positive and negative plate packs), a battery manufactured with a Pb–2.5 wt% Sn alloy may have 96 plates. This means that the pole will be from 200 to 300 g lighter than a similar one manufactured with a Pb–1 wt% Sn alloy. It is expected a volume of automotive batteries (battery size up to 60 Ah) in the European market in 2009 of about 60 million units [38]. The world's production of automotive lead-acid batteries will be from 5 to 10 times higher than that of Europe. These figures are strong indications that the use of a Pb–2.5 wt% Sn alloys for the manufacture of battery grids instead of a Pb–1 wt% Sn alloy can generate significant environmental and economical impacts.

4. Conclusions

Based on the present experimental electrochemical impedance parameters (EIS tests, anodic potentiodynamic polarization curves and equivalent circuit analysis) it can be said that coarse cellular structures tend to yield higher corrosion resistance than fine cellular morphologies for both as-cast Pb–1 wt% Sn and Pb–2.5 wt% Sn alloys. Such considerations are associated with the reduction of cellular boundaries of coarse cellular arrays when compared with finer cells, since the boundary has proved to be more susceptible to the corrosion action. In this context, the manufacturers of as-cast components of dilute Pb–Sn alloys can control the resulting microstructure cell size, as an alternative way to produce lead-acid battery components of higher corrosion resistance, by manipulating solidification processing variables. The use of a Pb–2.5 wt% Sn alloy for manufacturing battery grids may induce a single battery unit to be from 200 to 300 g lighter than a similar one manufactured with a Pb–1 wt% Sn alloy. If the annual world's production of automotive lead-acid batteries is considered the total saving in weight can have significant environmental and economical impacts.

Acknowledgements

The authors acknowledge financial support provided by FAPESP (The Scientific Research Foundation of the State of São Paulo, Brazil), FAEPEX – UNICAMP, and CNPq (The Brazilian Research Council).

References

[1] M.D. Achtermann, M.E. Greenlee, J. Power Sources 33 (1991) 87–92.
[2] J. Wirtz, Batteries Int. (January) (1996) 56.
[3] R.D. Prengaman, J. Power Sources 95 (2001) 224–233.
[4] R.D. Prengaman, in: K.R. Bullock, D. Pavlov (Eds.), Proceedings of the Vol. 84-14, Advances in Lead-Acid Batteries, The Electrochemical Society, Pennington, NJ, 1984, p. 201.
[5] R.D. Prengaman, J. Power Sources 158 (2006) 1110–1116.
[6] G.S. Al-Ganainy, M.T. Mostafa, F. Abd El-Salam, Physica B 348 (2004) 242–248.
[7] B. Rezaei, S. Damiri, J. Solid State Electrochem. 9 (2005) 590–594.
[8] M. Shiota, T. Kameda, K. Matsui, N. Hirai, T. Tanaka, J. Power Sources 144 (2005) 358–364.
[9] T. Hirasawa, K. Sasaki, M. Taguchi, H. Kaneko, J. Power Sources 85 (2000) 44–48.
[10] C.S. Lakshmi, J.E. Manders, D.M. Rice, J. Power Sources 73 (1998) 23–29.
[11] S. Stein, G. Bourguinon, L. Raboin, L. Broch, L. Johann, E. Rocca, Thin Solid Films 455–456 (2004) 735–741.
[12] E. Rocca, J. Steinmetz, Electrochim. Acta 44 (1999) 4611–4618.
[13] W.R. Osório, C.S.C. Aoki, A. Garcia, Mater. Sci. Forum 595–598 (2008) 851–859.
[14] W.R. Osório, P.R. Goulart, G.A. Santos, C. Moura Neto, A. Garcia, Metall. Mater. Trans. A 37 (2006) 2525–2537.
[15] W.R. Osório, D.M. Rosa, A. Garcia, J. Power Sources 175 (2008) 595–603.
[16] D.M. Rosa, J.E. Spinelli, W.R. Osório, A. Garcia, J. Power Sources 162 (2006) 696–705.
[17] W.R. Osório, C. Aoki, A. Garcia, J. Power Sources 185 (2008) 1471–1477.
[18] L.C. Peixoto, W.R. Osório, A. Garcia, J. Power Sources 192 (2009) 724–729.
[19] D. Pavlov, M. Bojinov, T. Laitinen, G. Sundholm, Electrochim. Acta 36 (1991) 2087–2092.
[20] D. Pavlov, M. Bojinov, T. Laitinen, G. Sundholm, Electrochim. Acta 36 (1991) 2081–2086.
[21] D. Pavlov, B. Monahov, G. Sundholm, T. Laitinen, J. Electroanal. Chem. 305 (1991) 57–63.
[22] F. Mansfeld, M.W. Kendig, J. Electrochem. Soc. 135 (1998) 828–835.
[23] J. Pan, D. Thierry, C. Leygraf, Electrochim. Acta 41 (1996) 1143–1153.
[24] M. Kliskic, J. Radosevic, S. Gudic, M. Smith, Electrochim. Acta 43 (1998) 3241–3255.
[25] M. Aziz-Kerrzo, K.G. Conroy, A.M. Fenelon, S.T. Farell, C.B. Breslin, Biomaterials 22 (2001) 1531–1538.
[26] S. Gudic, J. Radosevic, M. Kliskic, Electrochim. Acta 47 (2002) 3009–3016.
[27] S.L. Assis, S. Wolynec, I. Costa, Electrochim. Acta 51 (2006) 1815–1819.
[28] W.R. Osório, N. Cheung, J.E. Spinelli, P.R. Goulart, A. Garcia, J. Solid State Electrochem. 11 (2007) 1421–1429.
[29] W.R. Osório, P.R. Goulart, A. Garcia, Mater. Lett. 62 (2008) 365–369.
[30] D.Q. Martins, W.R. Osório, M.E.P. Souza, R. Caram, A. Garcia, Electrochim. Acta 53 (2008) 2809–2817.
[31] A. Cremasco, W.R. Osório, C.M.A. Freire, A. Garcia, R. Caram, Electrochim. Acta 53 (2008) 4867–4875.
[32] W.J. Lorenz, F. Mansfeld, Corros. Sci. 21 (1981) 647–672.
[33] W.R. Osório, L.C. Peixoto, L.R. Garcia, A. Garcia, Acta Metall. Sin., in press.
[34] A. Li, Y. Cheni, H. Chen, D. Shu, W. Li, H. Wang, C. Dou, W. Zhang, S. Chen, J. Power Sources 189 (2009) 1204–1211.
[35] D.M. Rosa, J.E. Spinelli, I.L. Ferreira, A. Garcia, J. Alloys Compd. 422 (2006) 227–238.
[36] W.R. Osório, C.M.A. Freire, A. Garcia, J. Alloys Compd 397 (2005) 179–191.
[37] P. Simon, N. Bui, N. Pebere, F. Dabosi, L. Albert, J. Power Sources 55 (1995) 63–71.
[38] J.F Dempwolff, Eurobat Automotive Battery Committee, EU Market Data 2007, accessed in website http://www.eurobat.org/documents.